JMEPEG (2009) 18:746–753
DOI: 10.1007/s11665-009-9433-7

1059-9495/$19.00

Shape Memory Alloy Tension/Compression Device for Seismic Retrofit of Buildings

Matthew Speicher, Darel E. Hodgson, Reginald DesRoches, and Roberto T. Leon

(Submitted September 16, 2008; in revised form February 20, 2009)

A tension/compression device is developed for applications as bracing elements in buildings. The device is designed to allow Nitinol forms, such as helical springs or Belleville washers, to be used in compression. The device allows both overall extension (tension) and compression while subjecting the Nitinol to an optimum deformation mode. It is possible, due to the versatility of the design, to adjust the force and stroke of the device without changing the overall configuration. This new device is subjected to a cyclic loading protocol that tests the Nitinol element's ability to recover large deformations. The effect of different Nitinol configurations and a cyclic loading history are evaluated in the study. The results show that Nitinol helical springs produce good recentering and damping behavior while Nitinol Belleville washers show good potential to form the basis for a Nitinol damping device.

Keywords Belleville washer, damper, NiTi, Nitinol, seismic retrofit, SMA

1. Introduction

Numerous researchers have investigated the use of recentering systems to improve the performance of structures during seismic events. The 2008 Sichuan Earthquake in China was a reminder of how a large portion of today's infrastructure is vulnerable to damage from earthquakes. One strategy to improve performance of buildings is to create systems that have the ability to recenter. In comparison to traditional passively damped systems, recentering systems have been shown to have at least equivalent performance (Ref 1, 2). Recentering systems can be broken down into two categories: (1) post-tensioned (PT) based systems and (2) shape memory alloy (SMA) based systems. PT systems use cables or elements to provide a restoring force during and after a loading event. Research on these systems first began in concrete buildings (Ref 3) and then was expanded to steel framed structures (Ref 4-7). These systems are often combined with supplemental damping to improve their performance.

SMA-based systems take advantage of the material's unique ability to recover large strains due to a solid-solid phase transformation and dissipate energy because of the resulting internal friction. For civil engineering, NiTi SMAs, otherwise know as Nitinol, have become the most popular SMA due to its favorable properties including hysteretic damping, large strain recovery, and excellent corrosion resistance. From a micro-scale to a macro-scale, Nitinol shows great promise for its use in seismic resisting systems (Ref 8). Nitinol SMA is the material which is evaluated in this paper.

A variety of research initiatives have looked at SMAs' viability as a structural recentering and damping element for both bridges and buildings (Ref 9). Dolce et al. (Ref 10) devised several types of recentering systems using SMA wires. They tested some devices which produced predicable behavior with good energy dissipation and excellent recentering. However, none of these devices have become widely used. In addition, other SMA-based systems have been investigated without wide implementation such as a self-centering friction damped brace by Zhu and Zhang (Ref 11) and beam-column connections by Ocel et al. (Ref 12), Penar (Ref 13), and Sepulveda et al. (Ref 14).

The inherent advantage of using an SMA-based system is that it can be designed to have (1) the ductility and energy dissipation to prevent collapse and (2) the ability to significantly reduce the residual deformations after an earthquake occurs. This research presents the development and initial testing of a new device that facilitates the use of two forms of Nitinol SMA: helical springs and Belleville washers. Whether the device is in tension or compression, the SMA elements are compressed. In addition, the device can use a wide array of shapes as the active components, which have a tremendous range of possible force and deformation characteristics.

2. Tension/Compression Device Description

The tension/compression device is a cylindrical-shaped damper that provides the ability to test a variety of SMA

This article is an invited paper selected from presentations at Shape Memory and Superelastic Technologies 2008, held September 21-25, 2008, in Stresa, Italy, and has been expanded from the original presentation.

Matthew Speicher, Reginald DesRoches, and **Roberto T. Leon**, School of Civil Engineering, Georgia Institute of Technology, 790 Atlantic Drive, Atlanta, GA 30332-0355; and **Darel E. Hodgson**, Nitinol Technology, Inc., 740-D Sierra Vista Ave., Mountain View, CA 94043. Contact e-mails: matthew.speicher@ce.gatech.edu, darel@nititech.com, reginald.desroches@ce.gatech.edu, and roberto.leon@ce.gatech.edu.

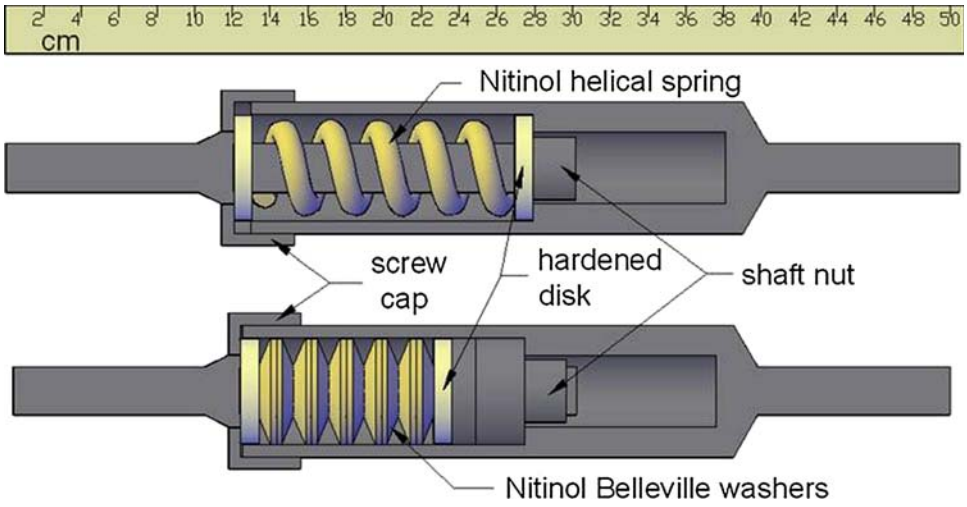

Fig. 1 Internal view of tension/compression device

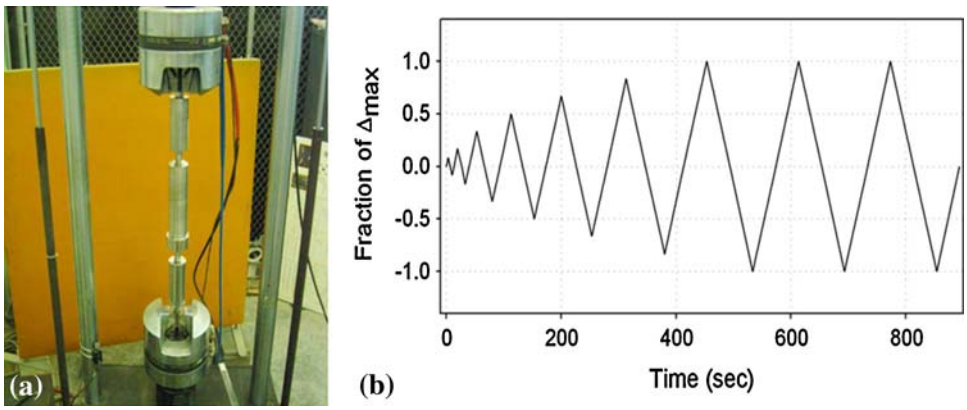

Fig. 2 (a) Test machine setup and (b) example loading protocol

elements. The body and the shaft of the device are made out of standard 304 stainless steel cylinders. Drawings of the device are shown in Fig. 1. The device is approximately 50 cm in length and 6.4 cm in diameter. The stroke capacity of the damper is dependant on the active element that is inserted, with values in the range of 2-5 cm for the devices presented in this paper. The damper is fitted with either helical springs or Belleville washers for the testing. Different strength and stiffness properties can be easily obtained by using different combinations of these elements. Two different springs and three different arrangements of Belleville washer are investigated.

3. Experimental Setup

An experimental scheme is devised to assess the viability of the SMA-based device using a 250 kN MTS Universal Testing Machine shown in Fig. 2(a). The MTS machine is fitted with hydraulic vee-notched wedge grips which can accommodate a rod diameter up to 1.9 cm. Stainless steel coupler elements are used to transfer the force from the 2.54 cm diameter rods of the damper to 1.9 cm diameter rods gripped by the MTS machine. The MTS machine is run by a Teststar controller running Testware software. The tests are conducted in displacement control using the built-in LVDT attached to the bottom grip.

A far-field loading protocol modeled after the protocol used in the SAC Steel Project (Ref 15) was selected for the experiments. The loading protocol, shown in Fig. 2(b), uses the testing machine's stroke as the deformation parameter. For each specimen arrangement, the maximum deformation was calculated and then 90% of this value was set as the target test maximum to prevent overloading of the device. A quasi-static loading rate for the testing was set at 0.127 cm/s to eliminate dynamic effects. Additionally, all experiments were carried out under ambient temperatures in the range of 26-28 °C. Self heating was not recorded because of the difficulty in monitoring the heat in the confined device and it was not expected to greatly impact the tests due to the quasi-static protocol implemented.

The tension/compression device was fabricated to facilitate the ability to implement different types of active elements.

In this paper six different tests are presented. The tests performed are as follows:

A. Cyclic protocol using the damper loaded with a hollow NiTi spring.
B. Cyclic protocol using the damper loaded with a solid NiTi spring.
C. Monotonic protocol compressing individual NiTi Belleville washers.
D. Cyclic protocol using the damper loaded with a single stack of 10 NiTi Belleville washers.
E. Cyclic protocol using the damper loaded with a double stack of 12 NiTi Belleville washers.
F. Cyclic protocol using the damper loaded with a triple stack of 12 NiTi Belleville washers.

4. Active Elements

Three different types of active elements are used for testing: a hollow spring, a solid spring, and a set of Belleville washers. The hollow NiTi spring has a diameter of 3.81 cm, an initial length of 14.20 cm, and a deformation capacity of 7.95 cm. The hollow spring was made from tubing with an outside and inside diameter of 12.5 and 9.5 mm, respectively. The solid SMA spring has a diameter of 3.81 cm, an initial length of 12.98 cm, and a deformation capacity of 4.57 cm. The solid spring was made from solid stock with a 12.5 mm diameter. The springs were made from Nitinol Alloy 508 (50.8% at.% Nickel). Both springs were made by heating small sequential sections of the stock with a small torch just to the point of initial softening (very low red heat, ~650-700 °C). The softened metal was then bent around a mandrel to produce a helix. The finished coils were given a final heat treatment to achieve uniform properties and good superelasticity.

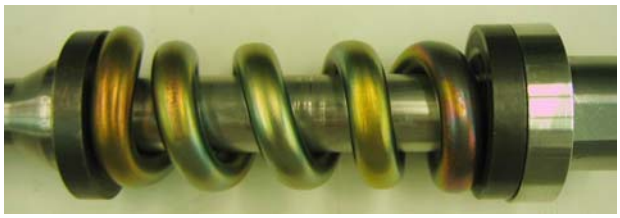

Fig. 3 Nitinol spring loaded on center shaft

The NiTi Belleville washers are 5.50 cm wide, 0.64 cm tall, and 0.305 cm thick. They were cut with a waterjet from a hot-rolled sheet of standard Nitinol Alloy 508. The conical shape was made by using a 30° angled cone. This yielded washers with a 26-27° angle. The same set of 12 washers is used for all the testing in this paper excluding washer 3 in the individual tests (test C). Washer 3 was from a set given a different heat treatment that yielded a higher transformation temperature resulting in reduced superelasticity. Additionally, a set of pretests were performed on these washers which is not presented in this paper.

5. Results of Helical Spring Tests

5.1 Hollow Helical Spring

Test A was performed using the hollow NiTi spring as the active element. The spring was inserted into the device and the shaft nut was tightened to give the spring 4.14 cm of precompression (Fig. 3). This was done to increase the initial stiffness of the device and to give a good flag-shaped hysteresis. The precompressed length of the spring was 10.06 cm and the fully compressed length was estimated at 5.83 cm. This resulted in a maximum device stroke of 4.23 cm to bring the spring loops into contact with each other. For the tests, 90% of this value (3.81 cm) was used as the test target maximum deformation. Using the previously described protocol, the resulting force-deformation plot was obtained (Fig. 4).

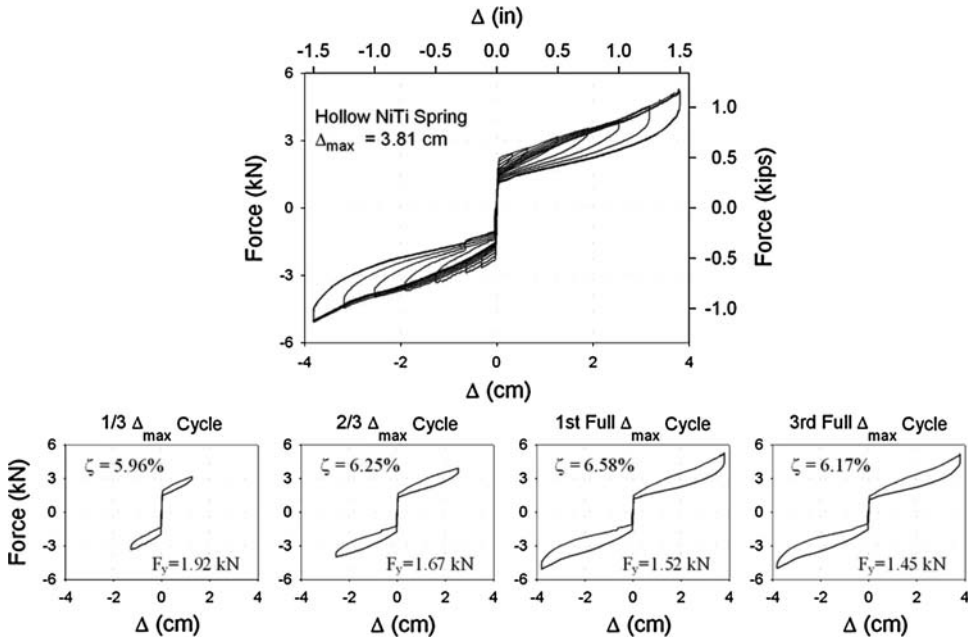

Fig. 4 Force-deformation response of hollow Nitinol spring in device (test A)

The 1/3, 2/3, and Full Δ_{max} cycles are highlighted to show the progressive behavior. The precompressed helical spring provided high initial stiffness and recentering over the entire cyclic protocol.

5.2 Solid Helical Spring

Test B was performed using the solid NiTi spring as the active element. Again the spring was inserted into the device and the shaft nut was tightened to give the spring 1.15 cm of precompression. The spring was only precompressed this amount because of how the spring fit on the shaft. The precompressed length of the spring was 11.83 cm and the fully compressed length was estimated at 6.75 cm. This resulted in a maximum device stroke of 5.08 cm; in which 90% of this value (4.57 cm) was used for testing. The cyclic loading protocol was applied and a similar quantitative behavior as the hollow spring was observed. The force-deformation curves are shown in Fig. 5, with the 1/3, 2/3, and Full Δ_{max} cycles individually displayed.

6. Discussion of Helical Spring Tests

The force-deformation relationships for both tests A and B demonstrate good hysteretic damping, limited strength degradation, and excellent repeatability. In assessing the performance of a damper, the equivalent viscous damping and the consistency of force levels are two important quantities. The equivalent viscous damping is defined as:

$$\zeta = \frac{E_D}{4\pi E_{so}} \quad \text{(Eq 1)}$$

where E_D is the energy dissipated in one cycle and E_{so} is the energy absorbed by an equivalent linear elastic system loaded to the same maximum force and displacement levels as used in E_D. In structural engineering, values of ζ around 5-10% are typical. For this paper, the yield force is defined as the force level in which the overall device breaks from its initial stiffness; which is the "kinked" point in the bilinear loading response. Also, the yield force is from the positive (tension) stroke of the device. Ideally this should not matter but in practice there was some difference between the positive and negative behavior. However, there was reasonable overall anti-symmetry observed.

The superelasticity combined with precompression of the spring resulted in a slender flag-shaped hysteric loop that accounted for ζ ranging from 6 to 11%, with the majority of the values between 6 and 7% for the hollow spring and 7 and 9% for the solid spring. In Fig. 6(a), the trend of ζ is graphically presented. In comparison to the solid spring, the hollow spring tended to have more stable levels of damping over the cyclic range.

When interpreting the behavior of the force levels in tests A and B, it should be noted that the precompression given to the hollow spring was almost four times that given to the solid spring. As a result, the hollow spring setup had a higher yield force than the solid spring, which at first glance is counterintuitive. However, the stiffness of the sloped loading plateau is clearly larger for the solid spring in comparison to the hollow spring. The yield forces for the hollow and solid springs are shown versus the fraction of Δ_{max} in Fig. 6(b). Both springs have the same trend; the yield force decreases as the loading cycles increase. The hollow spring yield force decreases faster than that of its solid counterpart. This can be contributed to the hollow spring having a larger precompression. When the cyclic loading is applied, the hollow spring is pushed further into its superelastic range which results in an increase in residual deformations due to accumulation of dislocations in the microstructure. This accumulation presets stress in the material causing a reduction in the yield force (Ref 16).

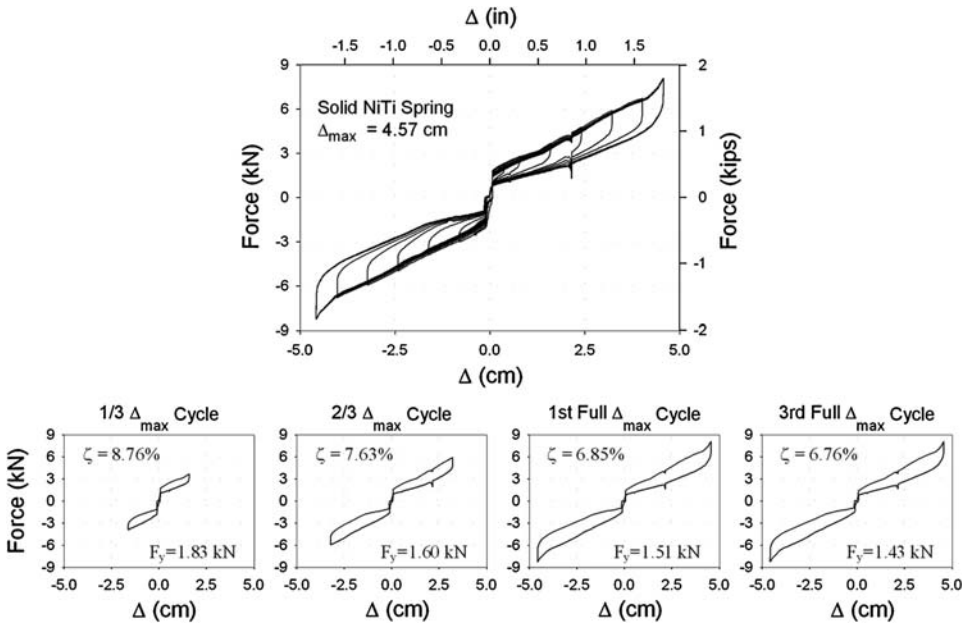

Fig. 5 Force-deformation response of the solid Nitinol spring in device (test B)

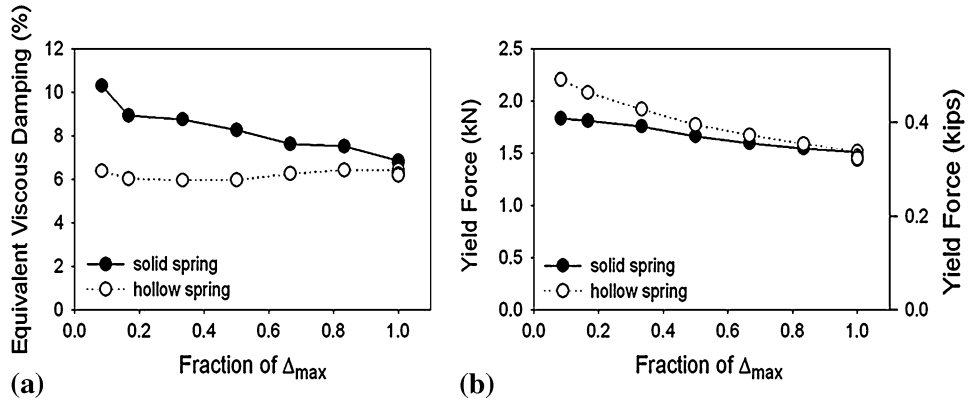

Fig. 6 (a) The damper's equivalent viscous damping and (b) yield forces over a range of deformations

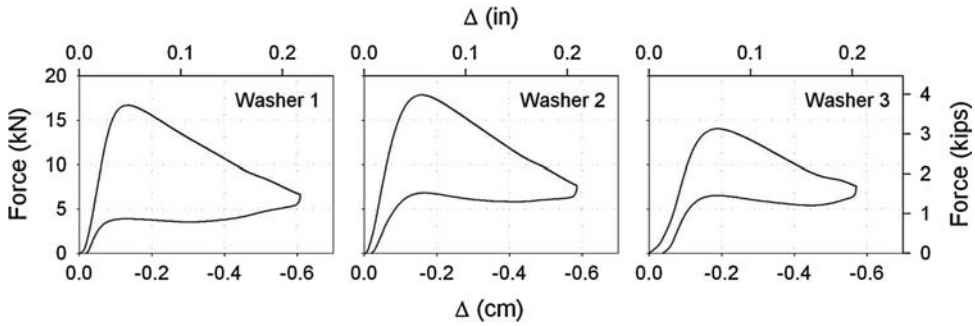

Fig. 7 Response of single NiTi Belleville washers under compression

7. Results of NiTi Belleville Washer Tests

7.1 Individual

In order to investigate the unknown behavior of the NiTi Belleville washers, three washers were randomly selected for compression testing (test C). These tests were performed in the MTS machine. The SMA Belleville washer was placed between two 1.27 cm hardened disks and compressed until just short of flat. The resulting duck-head-shaped force-deformation curves are shown in Fig. 7. The washers have good initial stiffness and strength, but at a deformation of approximately 0.15 cm the force carrying capacity peaks and there is a significant drop off until the imposed deformation is released at 0.605 cm. Washer 3 had the lowest strength and the highest residual deformation.

7.2 Single Stacked

Test D was conducted on a washer stack with the most flexible configuration of 10 singly stacked washers as shown in Fig. 8. Flat steel washers of 0.2 cm thickness were inserted between each SMA washer in an attempt to prevent the washers from inverting or buckling as seen in preliminary tests. As stated in the specimen description section, the SMA washers used in this test were not virgin; they had been used in preliminary tests.

The initial length and the test target maximum deformation of the washer configuration were 10.41 and 5.08 cm, respectively. The shaft nut was hand tightened. The resulting cyclic force-deformation curves are shown in Fig. 9. The washer stack gave semi-sporadic looking loading and unloading plateau

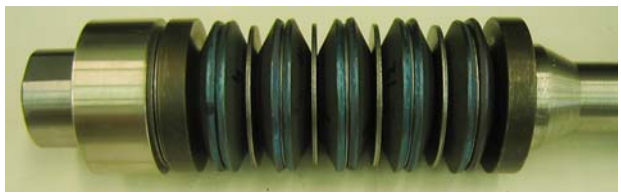

Fig. 8 Washer configuration for test D

tracks. The loading paths appeared to be repeatable and consistent. Some residual deformations were observed, especially as the cyclic loading got into larger deformations. After the test was complete and the damper was dissembled, it was observed that one of the washers had inverted. To recover its original shape, the washer was hit with a wooden mallet against a hard surface. The washer promptly snapped back.

7.3 Double Stacked

Test E was done using a double-stacked 12 washer configuration (Fig. 10), giving increased stiffness and strength in comparison to the single-stacked test. In this test, flat washers were not added in order to see if the double stack would naturally prevent individual washers from inverting. Additional stainless steel cylinders were added as fillers between the shaft nut and the hardened disk. Again the shaft nut was hand tightened and the cylinder was slid into position.

The initial length and test target maximum deformation of the washer configuration were 7.91 and 3.30 cm, respectively. The resulting force-deformation is shown in Fig. 11. A semi-sporadic

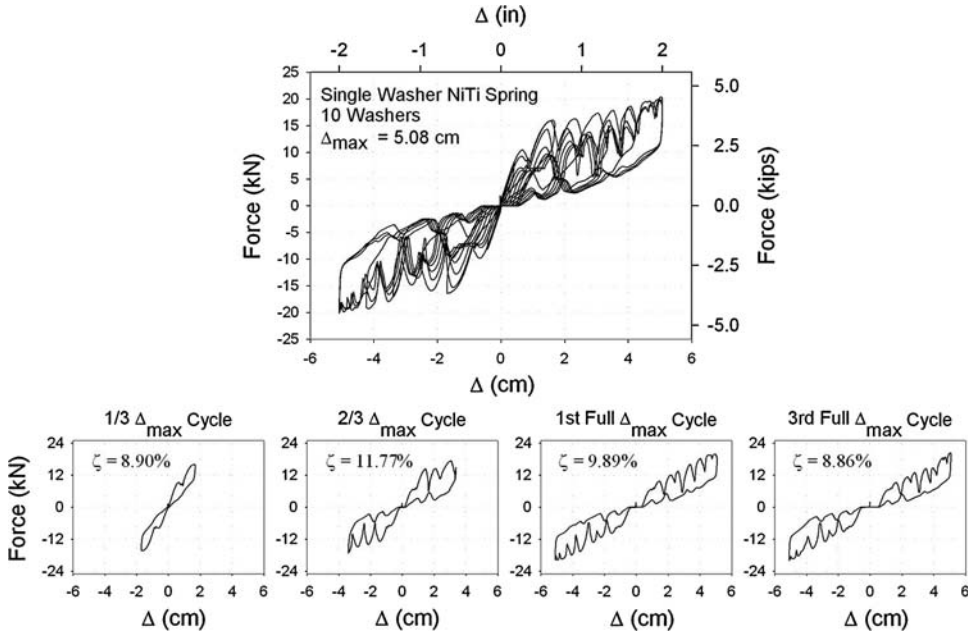

Fig. 9 Force-deformation response of single-stacked washer configuration (test D)

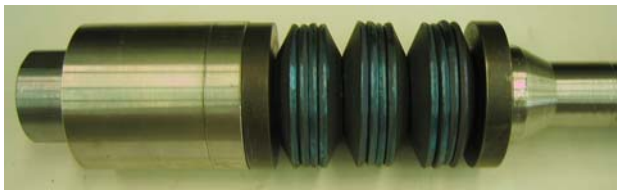

Fig. 10 Washer configuration for test E

response was observed, but this time fewer humps were noticed. After the test was complete and the damper was dissembled, one washer was found to be inverted. This washer was not the same one which inverted in the single-stacked test (test D).

7.4 Triple Stacked

The final test, test F, was done using a triple-stacked 12 washer configuration (Fig. 12), giving even more stiffness and strength in comparison to the double-stacked test. This time flat washers were again added to try to prevent the inverting

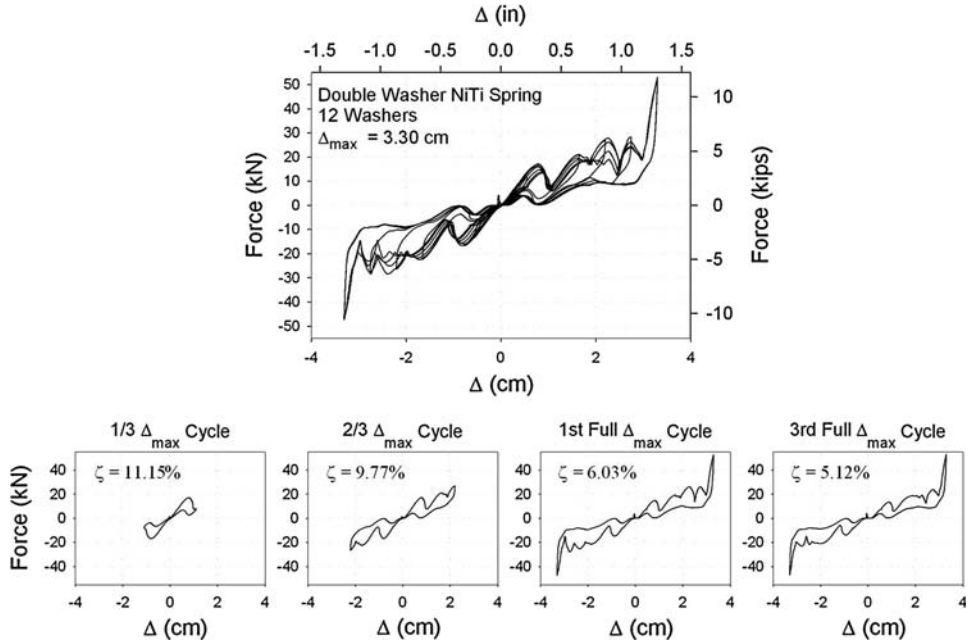

Fig. 11 Force-deformation response of double-stacked washer configuration (test E)

observed in the previous test. Additional stainless steel cylinders were added as fillers between the shaft nut and the hardened disk. Again the shaft nut was hand tightened and the cylinder was slid into position.

The initial length and test target maximum deformation of the washer configuration were 6.76 and 2.03 cm, respectively. The resulting force-deformation is shown in Fig. 13. This time a less sporadic load path was observed. The force-deformation curve had two distinct humps with a minor intermediate hump. After the test was complete and the damper was dissembled, no washers were found to be inverted.

8. Discussion of NiTi Belleville Washer Tests

8.1 Individual

As presented in the results section, the trend for all three individual washers were the same but there were varying levels of strength, stiffness, and residual deformations. The large initial stiffness followed by a peaking and falling off of load carrying capacity can be explained when looking at the geometry of the washer. A handbook (Ref 17) produced by Schnorr Corporation thoroughly details the behavior of Belleville washers made from Hookian elastic materials.

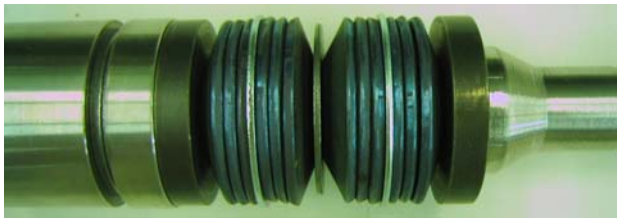

Fig. 12 Washer configuration for test F

Washers with similar geometry to those used in these tests show a response characteristic similar to Fig. 7, excluding the superelastic recovery seen during the release of the deformation. The effect of the superelasticity of the washer is not fully understood and more investigation is needed. However, when the washers were loaded to the flat position, some had the tendency to pass through a region of bifurcation and buckle into another stable configuration. After recovering the shape with a wooden mallet, no residual deformations were observed. Generally in structural engineering it is desired to have materials that retain load carrying capacity when subjected to large deformations, which is not the case here.

8.2 Single, Double, and Triple Stacked

The behavior of the single-stacked configuration was governed by the tendency of individual washers losing their load carrying capacity as they are deformed beyond a certain limit. This is the direct result of the duck-head-shaped behavior observed in the individual washer tests. Since each SMA Belleville washer can be assumed to have different peak strengths, the response of the single-stacked washer configuration is governed by the weakest link. As soon as the weakest washer is deformed to approximately 0.15 cm, this washer begins to loose its strength and thus take on the deformations of the other washers. This is reflected in the device's force-deformations humps. Once the displacement is increased enough to flatten the weakest washer, the remaining washers begin to pick up the force. This cycle is repeated until the entire group of washers has flattened or device deformation is decreased. Upon the release of the imposed deformation, the flattened Belleville washers spring back causing the force in the device to increase at moments even while the deformation is decreasing (see unloading path for Fig. 9, 11, and 13). The residual deformations of the setup begin to accumulate under the 2/3 Δ_{max} cycle. Upon the completion of the third Full Δ_{max} cycle, the residual deformation can be attributed to one

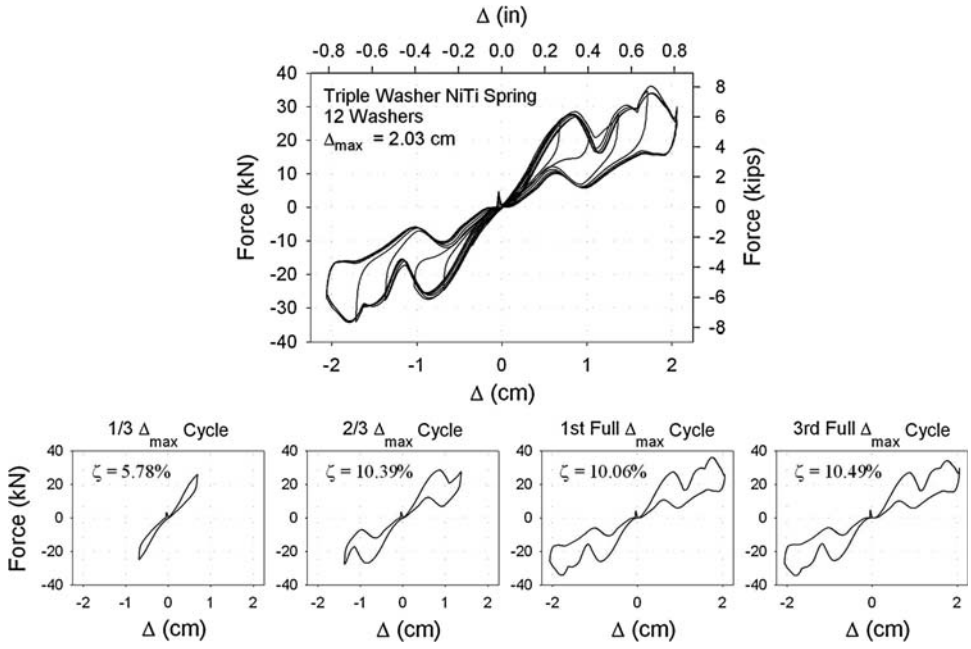

Fig. 13 Force-deformation response of triple-stacked washer configuration (test F)

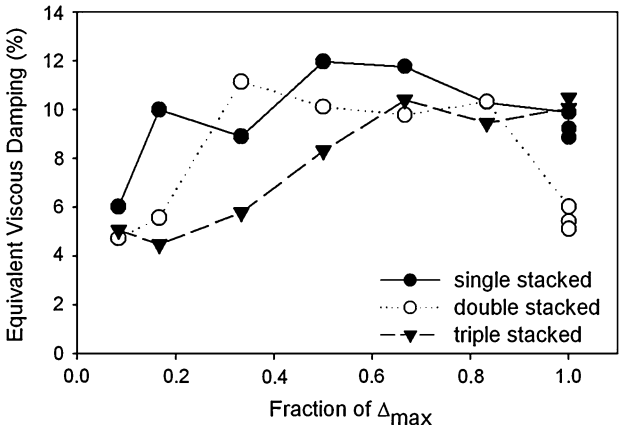

Fig. 14 Comparison of equivalent viscous damping ratios for the stacked washer tests

Belleville washer completely inverting as noted in the results section.

The double- and triple-stacked configurations had progressively less sporadic loading paths. Beyond the initial softness observed due to some of the washers settling into their positions, the stiffness increased as more washers were nested together. The initial stiffness, defined at a point half way up the first hump, was 1.74, 2.45, and 3.93 kN/mm for the single-, double-, and triple-stacked configurations, respectively. By adding more washers to each nest, fewer humps were able to form because there were fewer nests to allow this to occur. The drawback to the added stiffness and reduced hump count is the reduced deformation capacity. This could be improved by adding more nested washers to the stack, assuming one stays within the limitations of the device.

An important quantity to discuss is the equivalent viscous damping, ζ, of the stacked washer configurations. In Fig. 14, the ζ is compared for each washer test. The ζ ranged from just over 4% to just under 13%. The E_{so} was calculated by using the maximum deformation and the maximum force of each respective cycle (not necessarily the same point). The damping values were dependent on the location each deformation cycle fell in the humped response. The triple-stacked configuration showed increasing damping for increasing deformation. It was expected that for the more washers nested together, the more damping would be observed from the friction action between the nested surfaces. However, this was not clearly observed in the results.

9. Conclusions

Two SMA tension/compression devices were developed and tested with good initial results. In particular, the responses of the NiTi helical spring setups were promising because of the good superelasticity (as noted by the recentering), damping, and repeatability. More research needs to be done on the helical springs to determine if full scale load and stiffness levels can be achieved. The NiTi Belleville washers gave results that call for further development. Work needs to be done to develop washers that have improved individual force-deformation characteristics. These improvements should include creating washers that do not have the tendency to invert and also do not have the reduction in load carrying capacity as deformation is increased. Overall, the tension/compression device provides a convenient platform for implementing different forms of SMAs.

Acknowledgment

The authors thank Johnson Matthey for donating the stock NiTi materials for these experiments.

References

1. G.S. Cheok, W.C. Stone, and H.S. Lew, Seismic Performance Behavior of Precast Concrete Beam-Column Joints, *Proceedings of the Symposium on Structural Engineering in Natural Hazards Mitigation*, April 19–21, 1993 (Irvine, CA), p 83–88
2. J.M. Ricles, R. Sause, M.M. Garlock, and C. Zhao, Posttensioned Seismic-Resistant Connections for Steel Frames, *J. Struct. Eng.*, 2001, **127**(2), p 113–121
3. C. Christopoulos and A. Filiatrault, Post-Tensioned Energy Dissipating (PTED) Steel Frames for Seismic Regions, *2003 ASCE/SEI Structures Congress and Exposition: Engineering Smarter* (Seattle, WA), 2003, p 155–157
4. D.K. Nims, P.J. Richter, and R.E. Bachman, Use of the Energy Dissipating Restraint for Seismic Hazard Mitigation, *Earthq. Spectra*, 1993, **9**(3), p 467
5. J.M. Ricles, R. Sause, S.W. Peng, and L.W. Lu, Experimental Evaluation of Earthquake Resistant Posttensioned Steel Connections, *J. Struct. Eng.*, 2002, **128**(7), p 850–859
6. C. Christopoulos and A. Filiatrault, Seismic Response of Post-Tensioned Energy Dissipating Moment Resisting Steel Frames, *12th European Conference on Earthquake Engineering* (Como, Italy), 2002
7. C. Christopoulos, R. Tremblay, H.-J. Kim, and M. Lacerte, Self-Centering Energy Dissipative Bracing System for the Seismic Resistance of Structures: Development and Validation, *J. Struct. Eng.*, 2008, **134**(1), p 96–107
8. J. McCormick, J. Tyber, R. DesRoches, K. Gall, and H.J. Maier, Structural Engineering with NiTi. II: Mechanical Behavior and Scaling, *J. Eng. Mech.*, 2007, **133**(9), p 1019–1029
9. J.C. Wilson and M.J. Wesolowsky, Shape Memory Alloys for Seismic Response Modification: A State-of-the-Art Review, *Earthq. Spectra*, 2005, **21**(2), p 569–601
10. M. Dolce, D. Cardone, and R. Marnetto, Implementation and Testing of Passive Control Devices Based on Shape Memory Alloys, *Earthq. Eng. Struct. Dyn.*, 2000, **29**(7), p 945–968
11. S. Zhu and Y. Zhang, Seismic Analysis of Concentrically Braced Frame Systems with Self-Centering Friction Damping Braces, *J. Struct. Eng.*, 2008, **134**(1), p 121–131
12. J. Ocel, R. DesRoches, R.T. Leon, W.G. Hess, R. Krumme, J.R. Hayes, and S. Sweeney, Steel Beam-Column Connections Using Shape Memory Alloys, *J. Struct. Eng.*, 2004, **130**(5), p 732–740
13. B. Penar, "Recentering Beam-Column Connections Using Shape Memory Alloys," Masters Thesis, Georgia Institute of Technology, Atlanta, GA, 2004
14. J. Sepulveda, R. Boroschek, R. Herrera, O. Moroni, and M. Sarrazin, Steel Beam-Column Connection Using Copper-Based Shape Memory Alloy Dampers, *J. Constr. Steel Res.*, 2008, **64**(4), p 429–435
15. H. Krawinkler, A. Gupta, R. Medina, and N. Luco, Loading Histories for Seimsic Performance Testing of SMRF Components and Assemblies, *SAC/BD-00/10*, SAC Joint Venture, 2000
16. J.M. Gong, H. Tobushi, K. Takata, K. Okumura, and M. Endo, Cyclic Superelastic Deformation of TiNi Shape-Memory Alloy, *Mater. Sci. Forum*, 2000, **394–395**, p 245–248
17. E. Fromm and W. Kleiner. *Handbook for Disc Springs*, Schnorr Corporation, Hela Werbung, Hellbronn, 2003. http://www.schnorr.com/docs/Handbook.pdf